

FIGURE LIST :

1. Black particles in two-ball collision forward and backward
2. Three Geometries for generating shockwaves
3. 8192-particle twofold shockwave
- 4+5. Runge-Kutta Shockwave reversal—>Rarefaction
- 6+7. Shock forward and Shock backward important particles 2048
- 8+9 Rarefaction forward and backward important particles 2048
10. Thermodynamics of the 8192 rarefaction wave

Time-Symmetry Breaking in Hamiltonian Mechanics. II.

A Memoir for Berni Julian Alder [1925-2020]

William Graham Hoover with Carol Griswold Hoover

Ruby Valley Research Institute

601 Highway Contract 60

Ruby Valley, Nevada 89833

(Dated: October 16, 2020)

Abstract

This memoir honors the late Berni Julian Alder, who inspired both of us with his pioneering development of molecular dynamics. Berni's work with Tom Wainwright, described in the 1959 Scientific American[1], brought Bill to interview at Livermore in 1962. Hired by Berni, Bill enjoyed over 40 years' research at the Laboratory. Berni, along with Edward Teller, founded UC's Department of Applied Science in 1963. Their motivation was to attract bright students to use the laboratory's unparalleled research facilities. In 1972 Carol was offered a joint LLNL employee-DAS student appointment at Livermore. Bill, thanks to Berni's efforts, was already a Professor there. Berni's influence was directly responsible for our physics collaboration and our marriage in 1989. The present work is devoted to two early interests of Berni's, irreversibility and shockwaves. Berni and Tom studied the irreversibility of Boltzmann's "H function" in the early 1950s[2]. Berni called shockwaves the "most irreversible" of hydrodynamic processes[3]. Just this past summer, in simulating shockwaves with time-reversible classical mechanics, we found that reversed Runge-Kutta shockwave simulations yielded nonsteady rarefaction waves, not shocks. Intrigued by this unexpected result we studied the exponential Lyapunov instabilities in both wave types. Besides the Runge-Kutta and Leapfrog algorithms, we developed a precisely-reversible manybody algorithm based on trajectory storing, just changing the velocities' signs to generate the reversed trajectories. Both shocks and rarefactions were precisely reversed. Separate simulations, forward and reversed, provide interesting examples of the Lyapunov-unstable symmetry-breaking models supporting the Second Law of Thermodynamics. We describe promising research directions suggested by this work.

Keywords: Molecular Dynamics, Reversibility, Lyapunov Instability, Shock Waves, Rarefaction Waves

I. INTRODUCTION

Bill began to work with Berni in the fall of 1962. Over the next six years they published six joint works⁴⁻⁹, including one each with three coauthors: Francis Ree, Tom Wainwright, and Dave Young. All six works were motivated by Berni’s longstanding interest in understanding melting transitions for disks and spheres. The titles give an idea of their joint research: “Cooperative Motion of Hard Disks Leading to Melting”⁴; “Dependence of Lattice Gas Properties on Mesh Size”⁵; “Cell Theories for Hard Particles”⁶; “The Pressure, Collision Rate, and Their Number Dependence for Hard Disks”⁷; “High-Density Equation of State and Entropy for Hard Disks and Spheres”⁸; and last of all a longer review of their work, “Numerical Statistical Mechanics”, pages 79-113 in *Physics of Simple Liquids*⁹, edited by three of their friends and colleagues: Neville Temperley, John Rowlinson, and George Rushbrooke. These six papers can be found in the chronological publications list on our website, hooverwilliam.info, under “[The 1960s]”.

Besides introducing us to his worldwide colleagues Berni passed on cogent research advice: understanding is the goal; words and pictures are vital to understanding; equations, not so much; clarity of presentation is essential; of the three routes to understanding, formalism, experiment, and computation, at least two of these must be included and compared to make a publication “useful”.

Our goal in the present work is to shed more light on the connection of time-reversible atomistic dynamics to the irreversible Second Law of Thermodynamics. It is an extension of work with a similar title published in 2013¹⁰. Back then, we expressed our motivation:

“The goal we pursue here is improved microscopic understanding of the thermodynamic irreversibility described by the Second Law of Thermodynamics.”

In Section II we sketch three approaches to the irreversibility question: [1] the H Theorem, [2] fractal distributions from thermostatted systems, and [3] time-symmetry breaking through Lyapunov instability. Section III describes the example motivating the present work, a one-dimensional strong shockwave, simulated with classical manybody molecular dynamics. The shockwave study led automatically to an investigation of rarefaction waves. Sections IV and V detail the Lyapunov instabilities of both processes, shock and rarefaction, in both time directions, “forward” and “backward”. In both cases we develop and apply a novel precisely-reversible integration algorithm. Section VI describes the smooth-particle

technique for connecting the atomistic and continuum descriptions of flow problems, applied there to the measurement of longitudinal and transverse temperatures. A summary follows, in Section VII.

II. THREE EXPLANATIONS OF DYNAMICAL IRREVERSIBILITY

In 1956 Berni and Tom described several problems in their Brussels presentation “Molecular Dynamics by Electronic Computers”². Their evaluation of Boltzmann’s H Function, the 19th-century explanation of irreversibility, showed that low-density hard-sphere molecular dynamics and Boltzmann’s equation agreed quite well. In 1987 a second explanation of irreversibility from time-reversible dynamics¹¹ was offered as a consequence of Shuichi Nosé’s equilibrium thermostat ideas^{12,13} applied to nonequilibrium problems, following the progress of one- or two-dimensional particles through arrays of scatterers. The time-averaged temperature was controlled in the one-dimensional case¹⁴ and the instantaneous temperature was fixed in the two-dimensional case¹⁵. Both these problems supported a new explanation of irreversibility. Both generated fractal phase-space distributions with fractional dimensionalities less than that of the phase space. The rarity of nonequilibrium states, coupled with the exponential instability of the reversed fractal repeller motion, provided an explanation more general than Boltzmann’s. Rather than dilute gases the fractal description applied to a wide variety of liquid and solid problems¹¹.

In 2013 we made a third effort to understand irreversibility for manybody Newtonian systems through a novel measure of Lyapunov instability¹⁰. This pervasive instability can be followed by tracking the rate at which two nearby trajectories, the “reference” and the “satellite”, tend to separate, with the distance, but not the direction, between the two trajectories held fixed. The direction of the reference-to-satellite vector joining the two manybody trajectories determines which particles contribute most to the instability. **Figure 1** shows a striking difference between forward and backward analyses of an inelastic collision of two 400-particle balls¹⁰. The simulation is purely classical and precisely time-reversible. Forward in time the satellite particles most sensitive to instability (black in **Figure 1**) are those on the leading edges, those first to take notice of collision. When precisely the same trajectory is analyzed backward, with the 800-particle ball spontaneously (and completely unphysically) separating into its two parts, the “important particles” are very different.

Backward in time such particles are mostly in the high-strainrate necking region where new surfaces are being created. The forward collision is physically reasonable and can be simulated easily with a variety of integrators and algorithms, all of them leading to similar results. The reversed process, in which a single ball spontaneously separates into parts, is a different story, “irreversible”. It cannot be simulated directly. Instead it can only be studied by a brute-force numerical reversal of the forward-in-time collision.

III. SHOCKWAVES—THE “MOST IRREVERSIBLE” PROCESSES³

A comprehensive 1980 study¹⁶ examined the two shockwaves, with velocities $\pm u_s$, that result when a periodic liquid manybody system is suddenly compressed by two periodic images of itself. The left image advances rightward at the “piston velocity” $+u_p < u_s$. The right image leftward, at $-u_p$, propelling the faster shock with velocity $-u_s$. In the space of about two atomic diameters the argon liquid being modelled increases in pressure to 400 kilobars and in temperature to about ten thousand kelvins. The density increases approximately twofold.

Here we consider an alternative mechanism for shock generation, and in two space dimensions rather than three. See the middle illustration in **Figure 2**. We launch a stress-free cold solid against a fixed barrier at speed $u = u_p$. When complete, this process converts the initial macroscopic kinetic energy, $(Nu^2/2)$, into the internal energy of the resulting hot shocked fluid, Ne . We model the initial cold state with an N -particle triangular lattice, periodic in y . Each particle pair interacts with the short-ranged repulsive pair potential, arbitrarily normalized to unity:

$$\phi(r < 1) = (10/\pi)(1 - r)^3 ; \phi(r > 1) = 0 \rightarrow \int_0^\infty 2\pi r \phi(r) dr \equiv 1 .$$

In the present shockwave work N is either $8192 = 32 \times 256$ or $2048 = 16 \times 128$ so that the aspect ratio (L_x/L_y) , with close-packed columns of particles parallel to the y axis, is initially $8\sqrt{3/4} = 6.9282$. The shock propagation direction is parallel to the x axis.

The initial velocity, 0.97, is selected to shock-compress the cold solid twofold, to a hot fluid state. To break the lattice symmetry we begin with additional thermal velocities corresponding to an otherwise negligible temperature of 0.0001. **Figure 3** shows the coexistence of the hot shocked material with the cold stress-free triangular-lattice as modelled with 8192

particles. The number density ρ increases from $\sqrt{(4/3)}$ to $2\sqrt{(4/3)}$ and the internal energy change is consistent with the Hugoniot relation for twofold compression from the stress-free zero-energy cold state to a hot shocked state with temperature $T_H = 0.115$:

$$e_H - e_C \equiv (1/2)(P_H + P_C)(v_C - v_H) \text{ [Hugoniot Relation]}$$

$$\text{with } e_C = 0 \text{ and } P_C = 0 \text{ and } v_H = (v_C/2) \longrightarrow e_H = (1/2)P_H(v_C/2) = (1/2)P_H v_H .$$

$$\text{so that } e_H = P_H(0.433013/2) = 0.47045 = (0.97^2/2) \rightarrow P_H = 2.173.$$

To derive the Hugoniot relation imagine the cold zero-energy zero-pressure crystal moving rightward at speed $(0.97/2)$ and stagnating to match the velocity of a leftmoving wall at velocity $(-0.97/2)$. In this thought experiment the kinetic energy of the resulting leftmoving hot fluid is identical to that of the initial cold rightmoving solid, $(1/2)(0.97/2)^2$ per particle. Evidently the resulting internal energy e_H (the energy exclusive of the macroscopic motion) is identical to the per-particle work done by the crystal in the compression process, $(P_H v_H/2) = (0.97^2/2)$.

Just as in earlier work¹⁰ simulations show that the structures of such strong shockwaves are steady and accurately one-dimensional, with a shockwidth on the order of two particle diameters. In the shock-based coordinate system (fixed on the stationary shock, as shown in the top view of **Figure 2**) cold crystal enters from the left, with $u = u_s = 2u_p$, and exits at the right with $u = u_s - u_p = u_p = (u_s/2) = 0.97$. A time-reversal of this nonequilibrium shock process is easily implemented in a Runge-Kutta simulation by changing the sign of the timestep, $dt = 0.01 \rightarrow dt = -0.01$, or changing the signs of all the velocities in the problem.

Figures 4 and 5 illustrate the surprising result of this straightforward “reversal”. It motivated the present work. Rather than seeing the shock travel backward unchanged, at least for a reasonable time, instead we found that a rarefaction wave soon appears. Such a wave is typically generated by the nearly isentropic expansion of a compressed fluid and is discussed in standard fluid mechanics texts^{17,18} for simple fluid models. An accurate Leapfrog integrator, likewise conserving energy throughout the run to an accuracy of seven digits, produces a similar, likewise surprising, rarefaction. The “reversed motion” generated with either Runge-Kutta integration or Leapfrog is actually anything but! Notice the holes developing in the reversed solution. To investigate the mechanism for this convincing failure of algorithmic reversibility we turned to an analysis of the Lyapunov instability of the

process. We expected to see an analog of the symmetry breaking found for two colliding crystallites as shown in **Figure 1**. We will shortly discuss this investigation, in the next Section, IV. First we remind the reader how Lyapunov instability is characterized in numerical simulations^{19–21}.

A. Lyapunov Instability with a Satellite Simulation

The largest Lyapunov exponent identifies that part of a system in which the mechanics is least stable, with the highest growth rate of perturbations. It is evaluated in practice by following the progress of two neighboring trajectories, the “reference” and the “satellite”, rescaling their separation at the end of each timestep. The magnitude of this offset—here we use 0.0001—can be measured in coordinate q , momentum p , or (q, p) phase space. To carry out a precisely-reversed simulation one could use either Levesque and Verlet’s bit-reversible algorithm²² or our more-nearly-accurate implementation of one of Milne’s fourth-order algorithms¹⁰. Both these approaches express the particle coordinates as (large) integers. Typical force contributions, $\ddot{x}dt^2$ or $\ddot{y}dt^2$, become considerably smaller integers, but are still large relative to unity. Consistent floating-point computations of the force contributions, truncated to integers, then provide integer coordinate increments which are identical, apart from sign, in a pair of precisely-reversed motions.

B. A Simpler Time-Reversed Algorithm

For enhanced accuracy and simplicity we choose here a simpler time-reversible method of simulation, first storing an accurate Runge-Kutta reference trajectory for thousands of timesteps and then separately computing *two* nearby satellite trajectories, one forward and one reversed. The offset lengths of both satellite trajectories from the reference are returned from $|\delta(t)|$ to a fixed length δ_0 at the completion of each timestep, giving the instantaneous value of the largest Lyapunov exponent, $\lambda_1(t) \equiv \ln(|\delta(t)|/\delta_0)/dt$, for small dt , ± 0.01 in our simulations. All three trajectories, the reference and two satellites, are generated with the same Runge-Kutta integrator. A novel vital detail is that the positions of the satellite and reference trajectories often straddle a periodic boundary (in the y direction when the wave propagation direction is parallel to the x axis). To avoid discontinuous jumps in the

vector separating the two solutions it is necessary to detect and correct satellite coordinates which straddle the boundary, adding or subtracting L_y as the case may be, resulting in a continuously varying offset vector $\delta(t)$.

An interesting consequence of the Lyapunov analysis is that the (largest) Lyapunov exponent is uniformly positive in both time directions. Its numerical value is mostly in the range from 1 to 2 throughout both shockwave and rarefaction wave simulations. Insight into the Lyapunov instability of the motion comes from identifying which particles contribute most to the offset vector. In a pioneering effort Stoddard and Ford¹⁹ calculated the largest Lyapunov exponent of a Lennard-Jones fluid in 1967, maintaining the offset in coordinate space.

In 1998, with Kevin Boercker and Harald Posch²³, Bill simulated a nonequilibrium field-driven manybody particle flow and followed the largest local Lyapunov exponent, separately and instantaneously, in coordinate space and momentum space. The two identifications of the exponent’s “important particles” (those with above-average separations, $\delta_x^2 + \delta_y^2$ or $\delta_{p_x}^2 + \delta_{p_y}^2$), were very similar. Nearly all important particles in coordinate space were also important in momentum space, and *vice versa*. One could quantify a particle’s contributions to Lyapunov instability in at least three ways, in terms of

$$\delta_x^2 + \delta_y^2 \text{ or } \delta_{p_x}^2 + \delta_{p_y}^2 \text{ or } \delta_x^2 + \delta_y^2 + \delta_{p_x}^2 + \delta_{p_y}^2 .$$

Though different in principle²⁴, all three measures are in practice very similar in the particles they emphasize²³. **Figures 4 and 5** display the result of an important-particle Lyapunov analysis in coordinate space using the straightforward Runge-Kutta integrator, forward for 6000 timesteps and backward for another 6000, with $dt = \pm 0.01$. Here and in **Figures 6-9** we use 2048 particles rather than 8192 in order better to visualize details on an individual particle scale. **Figures 4 and 5** make the point quite convincingly that shockwaves are irreversible, even with very accurate integrators. Let us clarify the meaning of this observation by *storing* the (forward) evolution of the shockwave trajectory and then analyzing it for Lyapunov instability in both time directions.

IV. PRECISELY-REVERSIBLE SHOCK WAVE ANALYSES

Here **Figures 6 and 7** compare 2048-particle Lyapunov analyses forward and backward for the precisely-reversible (as the coordinates and momenta are all stored) simulations of that “most irreversible” shock process, the process shown in **Figure 3** for 8192 particles. The configurationally important particles have been colored brown in **Figures 4-9**. Notice that only in the reversed direction is the shockwave itself the maximally unstable portion of the system. Exactly the same configurations, when analyzed forward in time rather than backward, show that the shockwave is relatively stable (as opposed to unstable) *at* the shockfront. Maximal instabilities instead occur here and there throughout the hot fluid, in relatively small transient clumps when the propagation is analyzed forward in time. Similar clump formation was found in the field-driven motion analyzed in Reference 23. The difference in the location of “important particles” (backward in time, found at the shock, but forward in time, located in distant clumps) is a significant positive indication that Lyapunov analyses of Newtonian mechanics can provide a detailed understanding of the Second Law of Thermodynamics through the measurement of local instabilities. By including information local in space and time from past history the Lyapunov offset vectors, $\{ \lambda_1(t \pm dt) \longleftrightarrow \delta_1(t) \}$ quantify the simultaneous relative instabilities of microscopic motions. The difference found here between the forward and backward stability analyses of shocks is qualitative, not just quantitative, in the shockwave problem. We will come back to this analysis in our Summary section.

V. PRECISELY-REVERSIBLE RAREFACTION WAVE ANALYSES

In an effort to learn more here, we next generated, analyzed, and studied the evolution of instability in a rarefaction wave. Apparently the lower-density boundary condition in the reversed version of **Figure 5** provides an unnecessary perturbation of such a wave. To initiate a simpler pure-rarefaction simulation we first carry out an equilibrium Nosé-Hoover²⁵ isothermal high-density simulation (2048 particles with $\rho = 2\sqrt{(4/3)}$ and $T = 0.115$). The resulting equilibrated hot-fluid sample should allow us to start up a rarefaction simulation in a density-temperature state similar to that reached by the shockwave compression in the forward versions of **Figures 4 and 6**. Rather than using periodic boundaries in both the

x and y directions, as is usual in equilibrium situations, here we impose quartic boundary potentials, $dx^4/4$ at the left and right. These two smooth boundaries repel those particles venturing a distance dx beyond the limits $x = \pm(L_x/2)$. After equilibration, a rarefaction wave should result when we release one of the x boundaries. We choose to release the righthand boundary.

Figures 8 and 9 compare the forward and backward instability analyses of the resulting rarefaction wave. To make the details clear we again use only 2048 particles. The resulting wave was constructed with a three-step process, first simulating 20000 equilibration timesteps at the high-temperature high-pressure thermodynamic state reached earlier by shock compression. Next, the righthand boundary was released and the resulting expansion followed for 4000 Runge-Kutta timesteps, a time of 40. Finally, the velocities were reversed for a time of 40, returning to a close approximation of the initial high-temperature high-pressure state. This preliminary investigation surprised us yet again. Expansion (forming a rarefaction wave), followed by time reversal, showed no tendency toward shock formation. Instead the reversed flow closely approximated the rarefaction configurations. To analyze the motion precisely after equilibration, we followed and stored the 4000 $\{x, y, p_x, p_y\}$ rarefaction states, analyzing them in both directions so as to see the local “important particles”. **Figures 8 and 9** shows the important particles found in both time directions for the rarefaction wave. Here the unstable portions of both the forward and the backward rarefaction flows are all distributed in the hotter denser part of the wave. It is interesting, and was surprising to us, to see that reversing a rarefaction wave showed no tendency toward shockwave formation.

VI. CONTINUUM FIELD VARIABLES FROM (q, p) PARTICLE INFORMATION

Figure 10 displays thermodynamic data from the stored forward = backward trajectory of **Figures 8 and 9**. The velocities stored for the latter figure show no essential difference between the longitudinal and transverse temperatures, indicating that the rarefaction wave is indeed nearly isentropic. Such a wave provides the chance to measure the isentropic equation of state over a range of density and temperature. Let us do so now. We calculate “smoothed” values of the density and the longitudinal and transverse temperatures, $\{ \rho(x), T_{xx}(x), T_{yy}(x) \}$. To reduce fluctuations for **Figure 10** we use data for

8192 = 128 × 64 rather than 2048 particles. These data are smoothed with a properly normalized one-dimensional form of Lucy’s short-ranged smooth-particle weight function²⁶,

$$w(x, h) = (5/4hL)(1 - 6z^2 + 8z^3 - 3z^4) ; z \equiv (|x|/h) \rightarrow \int_{-\infty}^{+\infty} dx \int_{-L/2}^{+L/2} w(x)dy \equiv 1 .$$

$L = L_y$ is the height of the system. The weight function vanishes for $|x| > h$. In the initial hot fluid the 8192-particle system length was $L_x = 128\sqrt{(3/8)}$, reflecting both the spacing of close-packed triangular-lattice rows and a density twice the close-packed, $\rho_{\text{initial}} = 2\sqrt{(4/3)} = 2.3094$. The continuum number density at an x grid point $\rho(x_g)$ is given by the integrated density (delta functions) of particles nearby in their x coordinate, $\rho(x)$:

$$\rho(x_g) \equiv \sum_i^N w(x_i - x_g) \simeq \int_{-L/2}^{+L/2} dy \int_{x_g-h}^{x_g+h} w(x - x_g)\rho(x)dx .$$

The smoothing distributes the influence of each particle over a region of width $2h$ in x . The kinetic temperatures are given by similarly-averaged differences $\langle p^2 \rangle - \langle p \rangle^2$. **Figure 10** shows these local temperatures as functions of the local density for a smoothing length $h = 3$ at the conclusion of the rarefaction simulation. The plot approximates a straight line from the origin to the point $(\rho, T) = (2.3094, 0.115)$. Such a straight line corresponds to an ideal-gas isentrope, with the product $v \times T$ constant.

VII. SUMMARY AND SUGGESTED RESEARCH DIRECTIONS

Lyapunov analyses provide atomistic demonstrations and explanations of the symmetry-breaking instabilities associated with nonequilibrium states obeying standard classical mechanics. Developing robust algorithms for stationary shock and rarefaction waves is a worthy research goal. We encourage readers to consider these problems. A research goal stimulated by the present work is to quantify an instability metric. Such a metric would necessarily depend upon offset-vector components distinguishing the past from the future. Such a metric should also be related to entropy production and the Second Law of Thermodynamics.

A Lyapunov analysis of stationary states, as opposed to the transients treated here, is highly desirable. Steady-state shockwave simulations, with particles entering at the left and exiting at the right, just as in the stationary view of **Figure 2**, would make it possible to carry out longtime averages of instability properties. Most likely such an approach would assign to each particle in a variable-number system private forward and backward vectors,

both offset from the reference trajectory. These vectors would give pairs of private Lyapunov exponents, N forward and N backward at any time. Histories of these pairs could then be averaged to minimize fluctuations.

The continuum entropy production, depending as it does on gradients of thermodynamic properties, cannot distinguish between the two time directions. On the other hand the difference between the instability metrics forward and backward in time, because they depend only on their “pasts”, offers the chance better to quantify the relative stability of motions obeying and disobeying macroscopic thermodynamics.

VIII. ACKNOWLEDGMENTS

We very much enjoyed the chance to help honor Berni at his 90th Birthday Symposium at the Livermore Laboratory on 20 August 2015. In turn, Berni very kindly delivered the keynote address at Bill’s 80th Birthday Celebration at Sheffield the following year, on 26 July 2016. Our description of this pedagogical example of the irreversibility inherent in Newtonian dynamics was motivated in part by email correspondence with Marcus Bannerman and Kris Wojciechowski. We are grateful for their interest. We are grateful to the anonymous referee who pointed out some typographical errors in an earlier version of the manuscript and suggested that the direction of increasing time be indicated by arrows in Figures 4, 6, and 8.

-
- ¹ B. J. Alder and T. E. Wainwright, “Molecular Motions”, *Scientific American* **201**, 113-126 (1959).
- ² B. J. Alder and T. E. Wainwright, “Molecular Dynamics by Electronic Computers”, pages 97-131 in the Proceedings of the 27-31 August 1956 Symposium in Brussels, *Transport Processes in Statistical Mechanics*, edited by I. Prigogine (Interscience, New York, 1958).
- ³ M. Ross and B. Alder, “Shock Compression of Argon II. Nonadditive Repulsive Potential”, *Journal of Chemical Physics* **46**, 4203-4210 (1967).
- ⁴ B. J. Alder, W. G. Hoover, and T. E. Wainwright, “Cooperative Motion of Hard Disks Leading to Melting”, *Physical Review Letters* **11**, 241-243 (1963).
- ⁵ W. G. Hoover, B. J. Alder, and F.H. Ree, “Dependence of Lattice Gas Properties on Mesh Size”, *Journal of Chemical Physics* **41**, 3528-3533 (1964).
- ⁶ W. G. Hoover and B. J. Alder, “Cell Theories for Hard Particles”, *Journal of Chemical Physics* **43**, 2361-2367 (1966).
- ⁷ W. G. Hoover and B. J. Alder, “Studies in Molecular Dynamics. IV. The Pressure, Collision Rate, and Their Number-Dependence for Hard Disks”, *Journal of Chemical Physics* **46**, 686-691 (1967).
- ⁸ B. J. Alder, W. G. Hoover, and D.A. Young, “Studies in Molecular Dynamics. V. High-Density Equation of State and Entropy for Hard Disks and Spheres”, *Journal of Chemical Physics* **49**, 3688-3696 (1968).
- ⁹ B. J. Alder and W. G. Hoover, “Numerical Statistical Mechanics”, pages 79-113 in *Physics of Simple Liquids*, edited by H. N.V. Temperley, J. S. Rowlinson, and G. S. Rushbrooke, (North-Holland, Amsterdam, 1968).
- ¹⁰ W. G. Hoover and C. G. Hoover, “Time-Symmetry Breaking in Hamiltonian Mechanics”, *Computational Methods in Science and Technology* **19**, 77-87 (2013).
- ¹¹ B. L. Holian, W. G. Hoover, and H. A. Posch, “Resolution of Loschmidt’s Paradox: The Origin of Irreversible Behavior in Reversible Atomistic Dynamics”, *Physical Review Letters* **59**, 10-13 (1987).
- ¹² S. Nosé, “A Molecular Dynamics Method for Simulations in the Canonical Ensemble”, *Molecular Physics* **52**, 255-268 (1984).

- ¹³ S. Nosé, “A Unified Formulation of the Constant Temperature Molecular Dynamics Methods”, *Journal of Chemical Physics* **81**, 511-519 (1984).
- ¹⁴ W. G. Hoover, H. A. Posch, B. L. Holian, M. J. Gillan, M. Mareschal, and C. M. Massobrio, “Dissipative Irreversibility from Nosé’s Reversible Mechanics”, *Molecular Simulation* **1**, 79-86 (1987).
- ¹⁵ B. Moran, W. G. Hoover, and S. Bestiale, “Diffusion in a Periodic Lorentz Gas”, *Journal of Statistical Physics* **48**, 709-726 (1987).
- ¹⁶ B. L. Holian, W. G. Hoover, B. Moran, and G. K. Straub, “Shockwave Structure *via* Nonequilibrium Molecular Dynamics and Navier-Stokes Continuum Mechanics”, *Physical Review A* **22**, 2798-2808 (1980).
- ¹⁷ R. Courant and K. O. Friedrichs, *Supersonic Flow and Shock Waves* (Springer, New York, 1948 and 1999).
- ¹⁸ L. D. Landau and E. M. Lifshitz, *Fluid Mechanics* (Elsevier, Amsterdam, 1959 and 1987).
- ¹⁹ S. D. Stoddard and J. Ford, “Numerical Experiments on the Stochastic Behavior of a Lennard-Jones Gas System”, *Physical Review A* **8**, 1504-1512 (1973).
- ²⁰ I. Shimada and T. Nagashima, “A Numerical Approach to Ergodic Problems of Dissipative Dynamical Systems”, *Progress of Theoretical Physics* **61**, 1605-1616 (1979).
- ²¹ G. Benettin, L. Galgani, A. Giorgilli, and J. M. Strelcyn, “Lyapunov Characteristic Exponents for Smooth Dynamical Systems and for Hamiltonian Systems; a Method for Computing All of Them. Part 1: Theory”, *Meccanica* **15**, 9-20 (1980).
- ²² D. Levesque and L. Verlet, “Molecular Dynamics and Time Reversibility”, *Journal of Statistical Physics* **72**, 519-537 (1993).
- ²³ Wm. G. Hoover, Kevin Boercker, and H. A. Posch, “Large-System Hydrodynamic Limit for Color Conductivity in Two Dimensions”, *Physical Review E* **57**, 3911-3916 (1998).
- ²⁴ Wm. G. Hoover and C. G. Hoover, “Why Instantaneous Values of the ‘Covariant’ Lyapunov Exponents Depend upon the Chosen State-Space Scale”, *Computational Methods in Science and Technology* **20**, 5-8 (2014).
- ²⁵ W. G. Hoover, “Canonical Dynamics: Equilibrium Phase-Space Distributions”, *Physical Review A* **31**, 1695-1697 (1985).
- ²⁶ W. G. Hoover and C. G. Hoover, “SPAM-Based Recipes for Continuum Simulations”, *Computing in Science and Engineering* **3**(2), 78-85 (2001).

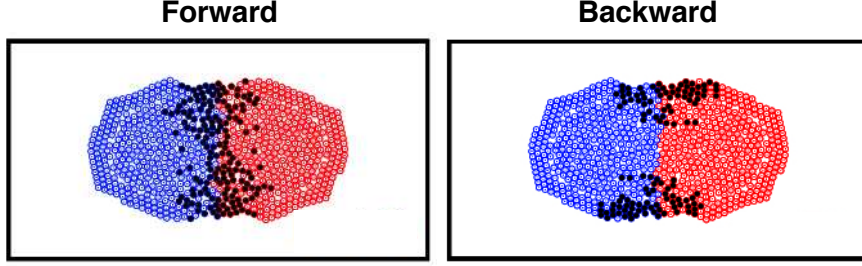


FIG. 1: Two identical snapshots from a “bit-reversible” precisely-time-reversible Newtonian collision of two solid 400-particle balls¹⁰. The important particles forward and backward in time show that local mechanical instability, not phase volume, is the mechanism for Second Law irreversibility.

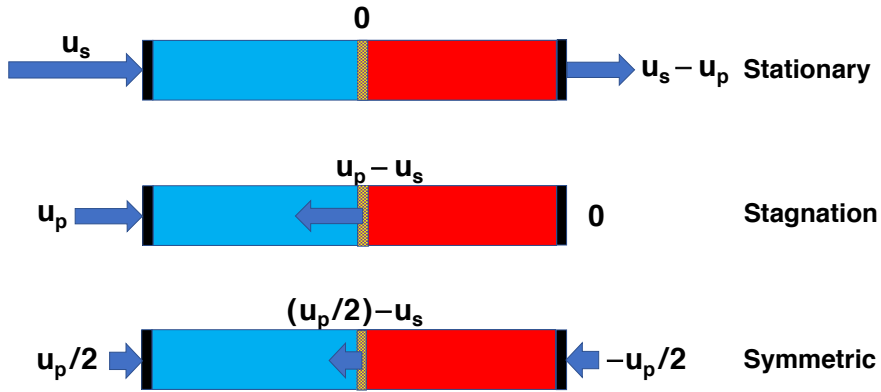


FIG. 2: Three mechanisms for generating one-dimensional shockwaves. We use stagnation geometry here. The symmetric mechanism leads to the Hugoniot Relation $\Delta e = \langle P \rangle \Delta v$, where $\langle P \rangle$ is the average of the cold and hot pressures and Δv is the difference of the cold and hot volumes.

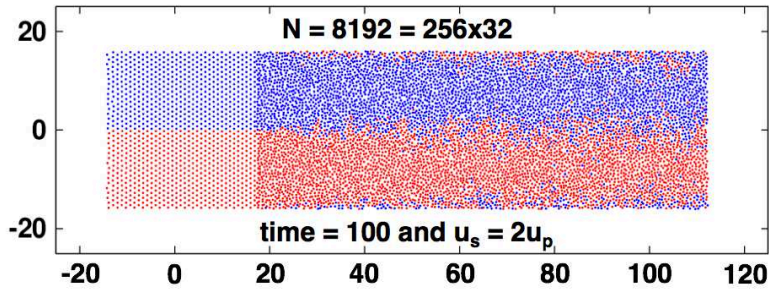


FIG. 3: A one-dimensional leftmoving shockwave. Initially cold solid at density $\sqrt{4/3}$ moves rightward at $u_p = 0.97$, stagnates at a fixed barrier at $x = 128\sqrt{3/4} = 110.85$, launches a twofold-compressed shockwave leftward, at $u_p - u_s = -0.97$. Colors show original y values. The timesteps in all of these simulations are equal to 0.01.

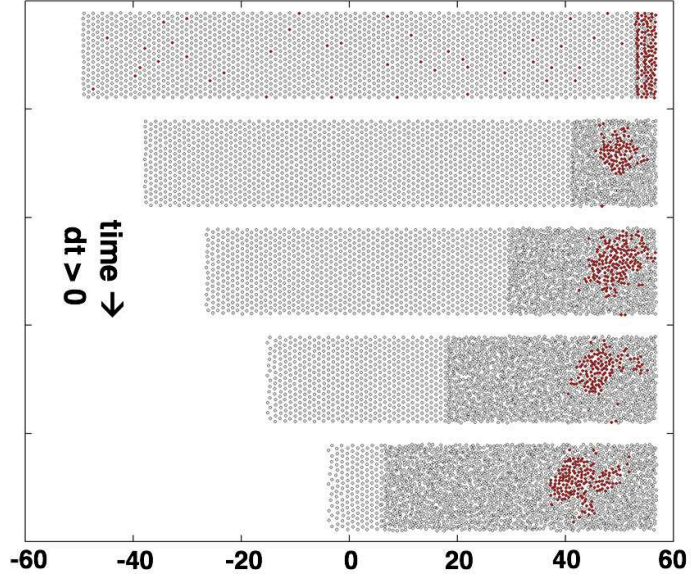


FIG. 4: Runge-Kutta shockwave forward in time. The original cold zero-energy zero-temperature specimen, moving rightward at speed 0.97, had a length of $128\sqrt{3/4}$ and a height of 16. There are 2048 particles with an initial nearest-neighbor spacing of unity. The snapshots taken forward in time correspond to times of 6, 18, 30, 42, and 54. The motion is reversed at time 60.

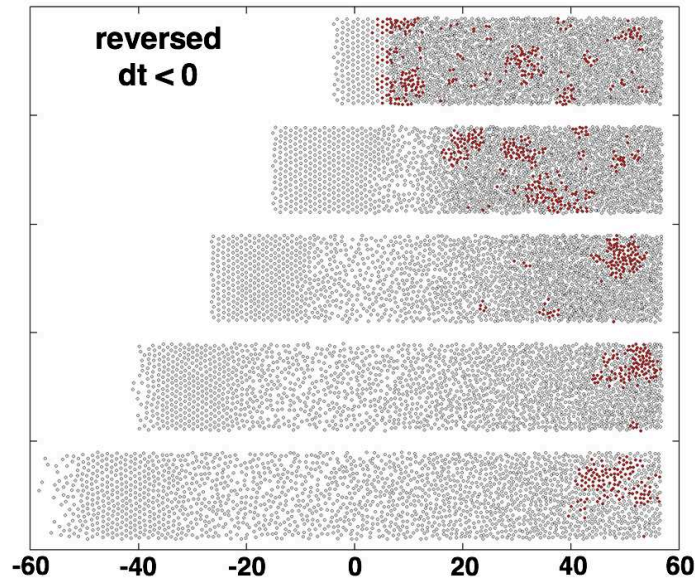


FIG. 5: Reversed Runge-Kutta shockwave breaks up and yields a rarefaction wave. Evidently the reversed shockwave structure is highly unstable. The times here correspond to those in Figure 4.

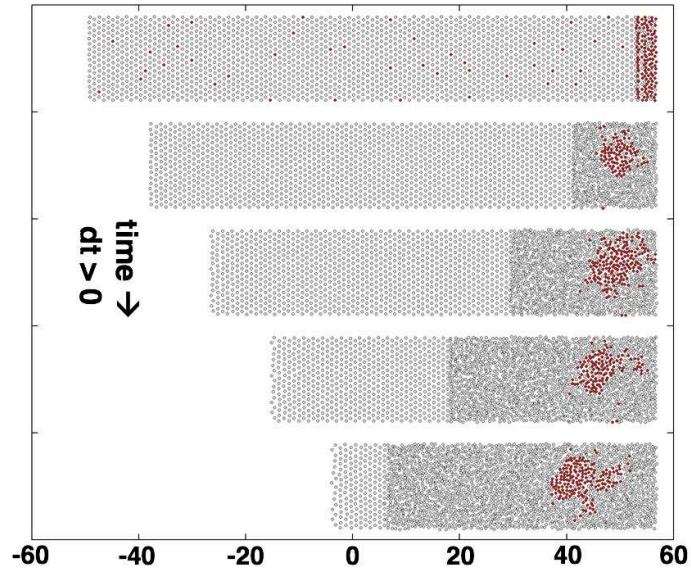


FIG. 6: A precisely reversible shockwave stored during propagation forward in time. Here the coordinates and momenta are stored, matching Figure 4. The reversed shockwave structure has been stored for use in Figure 7.

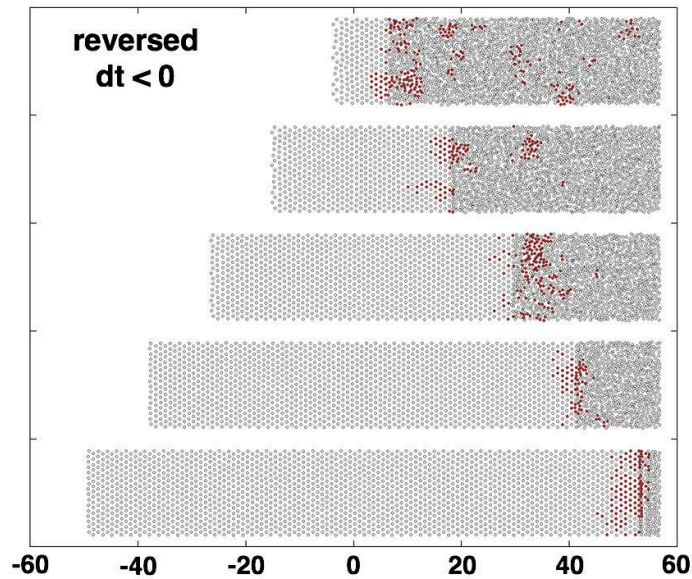


FIG. 7: The stored trajectory of Figure 6 is played backward, with the velocities reversed. Notice that the important particles, colored brown, are concentrated near the reversed shockwave, indicating its enhanced instability. After reversal at time 60 time decreases through the snapshot times of 54, 42, 30, 18, and 6.

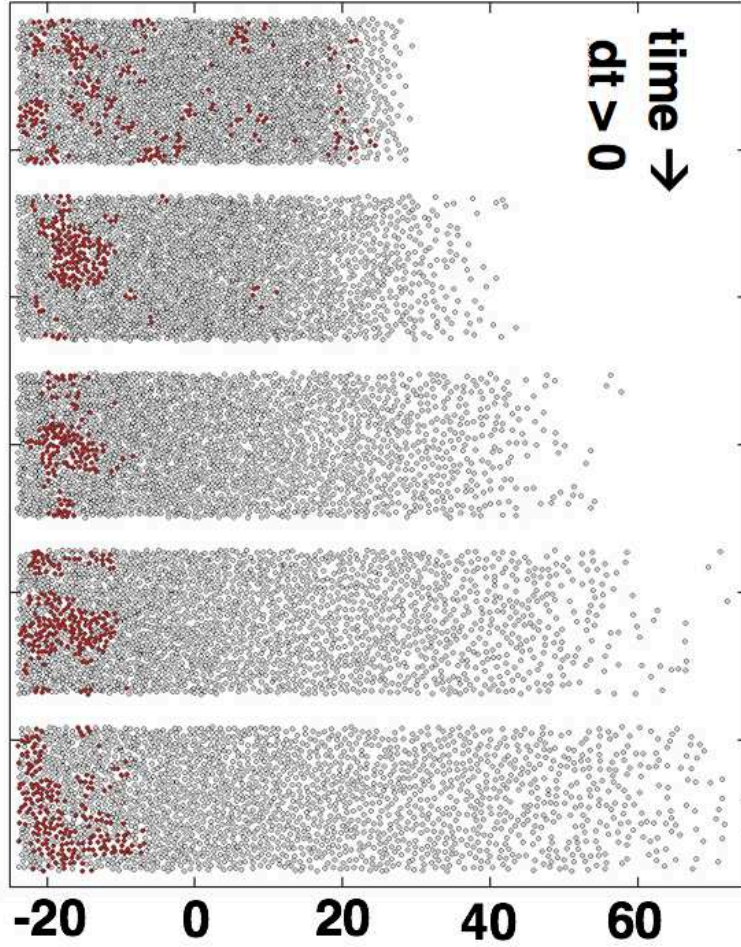


FIG. 8: Here and in Figure 9 snapshots at times of 4, 12, 20, 28, and 36 show that the important particles accumulate in clumps near the left wall, which feels the recoil pressure reacting to the rarefaction fan's motion to the right. Here the original length of the 2048-particle hot specimen, with temperature 0.115 and density $2\sqrt{4/3}$, was $32\sqrt{2}$ with height $8\sqrt{6}$. Unlike the shockwave problem the important particles in both time directions occur near the warmer lefthand boundary.

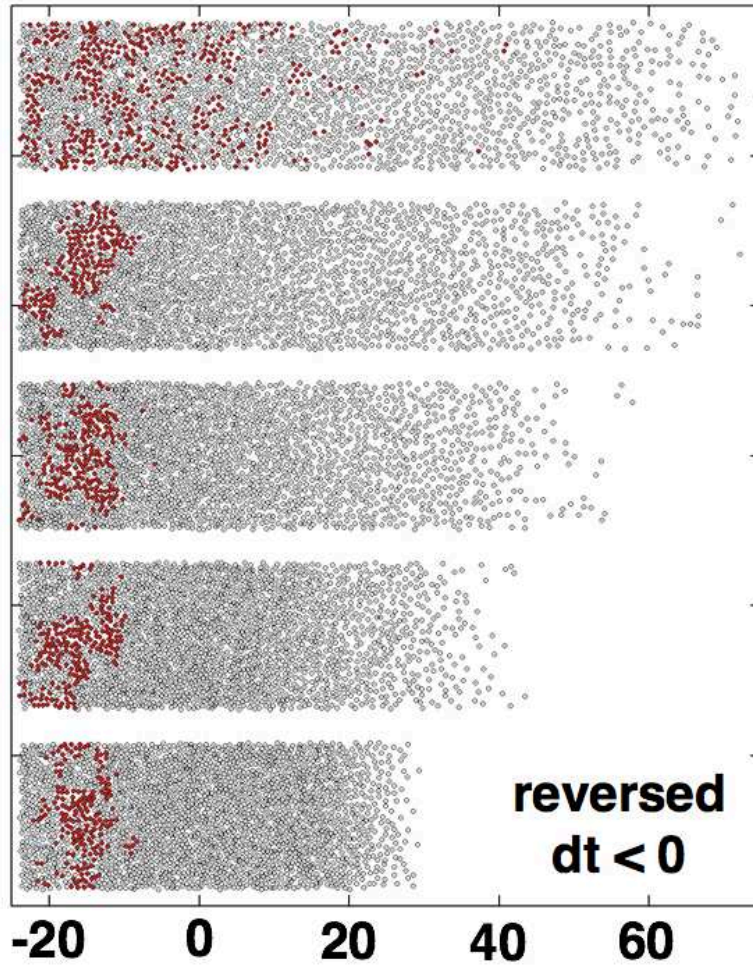


FIG. 9: The stored precisely-reversed rarefaction wave of Figure 8 analyzed backward in time. As before the important particles are colored brown.

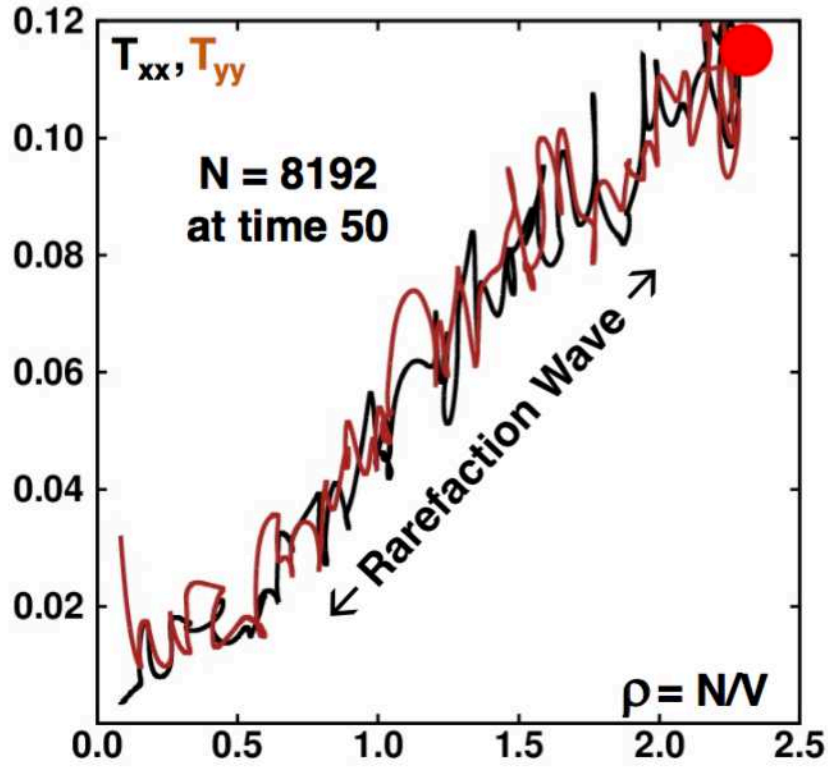


FIG. 10: Temperatures and Density in a Rarefaction Wave. To reduce fluctuations 8192 particles were used. The similarity of the longitudinal and transverse temperatures is remarkable. The red dot at the upper right indicates the initial thermodynamic state imposed by Nosé-Hoover dynamics.